Ionic Liquid–Assisted Hydrothermal Synthesis of Monoclinic Structured LaVO4 Nanowires through Topotactic Transformation from Hexagonal La(OH)3 Nanowires

ARTICLE *in* CRYSTAL GROWTH & DESIGN · DECEMBER 2009

Impact Factor: 4.89 · DOI: 10.1021/cg900887q

3 AUTHORS, INCLUDING:

Wenjun Zheng
Nankai University
112 PUBLICATIONS **2,290** CITATIONS

SEE PROFILE

DOI: 10.1021/cg900887q

CRYSTAL GROWTH & DESIGN Article

2010, Vol. 10 262–267

Ionic Liquid-Assisted Hydrothermal Synthesis of Monoclinic Structured $LaVO_4$ Nanowires through Topotactic Transformation from Hexagonal $La(OH)_3$ Nanowires

Yan Sun, Chunsheng Li, and Wenjun Zheng*

Department of Materials Chemistry and Key Laboratory of Energy-Material Chemistry (Tianjin), College of Chemistry, Nankai University, Tianjin 300071, People's Republic of China

Received July 28, 2009; Revised Manuscript Received November 10, 2009

ABSTRACT: Ultralong *m*-$LaVO_4$ nanowires were synthesized from *h*-$La(OH)_3$ nanowires via topotactic transformation in an ionic liquid-assisted hydrothermal system. The structure and morphology of the as-synthesized samples were characterized by X-ray diffraction, field emission scanning electron microscopy, transmission electron microscopy/high-resolution TEM, and Fourier transform infrared spectrometry. It was found that ionic liquid [BMIM]Br can effectively influence the morphology of *h*-$La(OH)_3$ one-dimensional nanostructures through the adsorbing model of [BMIM]Br on the (010) plane, which controlled the oriented growth along the [001] direction. After the results were systematically analyzed from products obtained by modifying the reaction time from 1 to 48 h, topotactic transformation from *h*-$La(OH)_3$ through the diffusion of VO_3^- ions to *m*-$LaVO_4$ is proposed to explain the growth mechanism of *m*-$LaVO_4$ nanowires.

1. Introduction

The controlled synthesis of one-dimensional (1D) inorganic nanomaterials are currently of high interest because the size and morphology impact both physical and chemical properties.[1] Among various wet-chemical techniques, ionic liquids (ILs) are widely used as structure-directing agent, solvents, and reactants to tailor the growth of 1D inorganic nanostructures.[2] Some researchers have demonstrated that a hydrogen bond-co-$\pi-\pi$ stack mechanism is crucial to control the shapes of nanoscale building blocks in ILs system.[3] Furthermore, our group has reported the hydrogen bond-co-$\pi-\pi$ stack interaction closely related to the surface structure of rutile TiO_2 nanoparticles and addressed an adsorbing model of ILs on the (110) plane of TiO_2.[4] However, an obvious problem still exists about the universality of the adsorbing model of ILs on the surface architectures of inorganic materials. One generally accepted strategy to solve the mentioned issue is to choose materials with a suitable surface structure to induce their 1D growth using an ILs-assisted process. Thus, we pay attention to the controlled synthesis of hexagonal (*h*-) $La(OH)_3$ 1D nanostructures, because the structure of *h*-$La(OH)_3$ along its *a* or *b* axis is in accordance with the hydrogen bond-co-$\pi-\pi$ stack interaction.

Metal vanadates, as one of the most attractive inorganic nanostructures, have numerous applications in the fields of high-energy power sources,[5] catalysts,[6] optical devices,[7] and magnetic materials,[8] etc. In particular, lanthanum orthovanadate ($LaVO_4$) is to be recognized as a functional material due to its layered structure and two polymorphs: monoclinic (*m*-) monazite type and tetragonal (*t*-) zircon type.[9] Recently, great progress has been made in the hydrothermal synthesis of *t*-$LaVO_4$ nanostructures[10−12] and the investigations in the improved luminescent behavior[10a−d,11] and catalytic activity.[10a,e] Nevertheless, only a few studies have been reported on the preparation of *m*-$LaVO_4$ nanomaterials.[10a,b,13,14] Therefore, it remains a great challenge to control the fabrication of ultralong *m*-$LaVO_4$ nanowires with uniform diameters. Until now, topotactic transformation process is widely involved the formation of 1D precursors into novel 1D nanostructures.[15] We attempt to produce the complex topotactic transformation from *h*-$La(OH)_3$ nanowires through the diffusion of VO_3^- ions to *m*-$LaVO_4$ nanowires on the basis of the similarity in their layered structures.

In this paper, we focus on an IL-assisted hydrothermal synthesis of ultralong *m*-$LaVO_4$ nanowires from *h*-$La(OH)_3$ via topotactic transformation. Our primary work can be summarized in two parts: To begin with, *h*-$La(OH)_3$ single-crystalline nanowires were generated using the ionic liquid 1-butyl-3-methylimidazolium bromide ([BMIM]Br) to effectively strengthen the 1D growth habit. Second, *m*-$LaVO_4$ wire-like nanostructures were successfully prepared through the topotactic transformation from the precursor $La(OH)_3$ nanowires by extending the reaction time.

2. Experimental Procedures

2.1. Synthesis. All chemicals were analytical grade and used without further purification. Ionic liquid [BMIM]Br was synthesized according to the procedures in the literature.[16] The reaction process is shown in Scheme 1.

The *m*-$LaVO_4$ nanowires were prepared through an ionic liquid [BMIM]Br-assisted hydrothermal route from the reactions among $La(NO_3)_3$, NH_4VO_3, and NaOH. Briefly, the chemical reactions are given in equations as follows:

$$NH_4VO_3 + NaOH \rightarrow NaVO_3 + NH_3\uparrow + H_2O$$

$$La(NO_3)_3 + 3NaOH \xrightarrow[1-8\ h]{200^\circ C} La(OH)_3\downarrow + 3NaNO_3$$

$$NaVO_3 + La(OH)_3 \xrightarrow[t>8\ h]{200^\circ C} LaVO_4\downarrow + NaOH + H_2O$$

In a typical procedure, 75.0 mmol of NaOH and 3.5 mmol of NH_4VO_3 were dissolved into 12.0 mL of distilled water, followed by

*Corresponding author. Fax: +86-22-23502458. E-mail: zhwj@nankai.edu.cn, juzi147@yahoo.com.cn.

 Published on Web 12/11/2009

the addition of a mixed solution of 1.5 mL of [BMIM]Br (0.01 M) and 7.5 mL of ethanol under stirring at room temperature. Then, 2.5 mmol of $La(NO_3)_3$ aqueous solution was added dropwise to the above solution with vigorous stirring and the solution turned a white suspension immediately. After continuous mixing for 15 min, the suspension was transferred into a 30 mL Teflon-lined stainless autoclave and heated at 200 °C for 1 to 48 h. As the autoclave cooled to room temperature naturally, the white powers were directly collected by centrifugation, washed with distilled water and absolute ethanol several times, and finally vacuum-dried at 80 °C for 6 h. The effect of the various amounts of [BMIM]Br and reaction temperatures were systematically investigated in the reaction system, but other parameters were kept constant. Heat treatment was carried out at 600 °C for 12 h in air condition to increase the purity of *m*-$LaVO_4$ nanowires for further characterization. Moreover, the experimental conditions with different reaction time were also investigated in order to understand the growth mechanism of ultralong *m*-$LaVO_4$ nanowires. Table 1 summarizes these typical conditions and the corresponding morphologies and phases evolution of the products.

2.2. Characterization. The X-ray diffraction (XRD) analysis was performed on a Rigaku D/max 2500 V/PC X-ray diffractometer equipped with Cu Kα radiation (λ = 1.54056 Å), while the voltage and electric current were held at 40 kV and 100 mA. The field emission scanning electron microscopy (FE-SEM) images were taken on a JEOL JSM-6700F scanning electron microscope at 10 kV, and TESCAN MIRA II-LMU at 20 kV. The transmission electron microscopy (TEM) and high-resolution transmission electron microscopy (HRTEM) images were obtained on a Philips Tecnai G2 F20 transmission electron microscope at an acceleration voltage of 200 kV. The samples were supported on carbon-coated copper grids by dropping the ethanol solution containing uniformly dispersed as-obtained samples. Fourier transform infrared spectrometry (FTIR) measurements were recorded with a Bruker Optics Instrument type Tensor 27 spectrophotometer.

3. Results and Discussion

3.1. Formation, Structure, and Morphology. The XRD pattern of sample prepared under hydrothermal conditions with [BMIM]Br (0.01 M) at 200 °C for 8 h (Figure 1a) indicates that all the peaks can be well assigned to $La(OH)_3$ with the hexagonal structure (JCPDS No. 36-1481, space group: *P*63/*m* (No. 176)). Figure 2a,b shows low- and high-magnification TEM images of *h*-$La(OH)_3$ nanowires. The diameter of the as-synthesized nanowires is about 8−9 nm with a length up to 600 nm. The HRTEM image in Figure 2c clearly reveals a lattice spacing of 0.318 nm corresponding to the (101) plane of *h*-$La(OH)_3$, indicating that the growth direction along the [001] direction with the dominant exposed surface being the (010) plane. For the (010) plane structure of *h*-$La(OH)_3$ in Figure 2d, the distances of ab (or cd) and ac (or bd) in the parallelogram are 0.625 and 0.619 nm, respectively. Fortunately, these distances are in the range of the mutual π-stacking distance (0.6−0.7 nm) between aromatic rings.[17] As demonstrated for the hydrogen bond-co-$\pi-\pi$ stack mechanism in our previous work,[4] $[BMIM]^+$ ions may vertically adsorb on the (010) plane via a *h*-$La(OH)_3$-p(3 × 1)-$[BMIM]^+$ original cell to construct a tight adsorption layer (Figure 2e). Moreover, the (010) plane composed of OH^- groups exhibits negative charges, while the (001) plane of *h*-$La(OH)_3$ is electrically neutral because it is built with the planar triangle formed one La^{3+} and three OH^- ions. Thus, $[BMIM]^+$ ions are favored to adsorb on the (010) plane with negative charges and then reduce the growth rates along the [010] direction, which causes the growth of *h*-$La(OH)_3$ along the *c* axis to reach the aim of 1D shaped-controllable synthesis.

In order to confirm the mentioned discussions, a comparative experiment was conducted on the absence of ionic liquid [BMIM]Br. The as-obtained *h*-$La(OH)_3$ product has a rod-like morphology with nonconstant diameters of 30−200 nm and an aspect ratio of over 10 (see Figure S1 in the Supporting Information). Although the obtained product still has a 1D growth habit, its shape homogeneity and aspect ratio are very inferior to the sample prepared with the addition of [BMIM]Br. The results agree well with the analysis of the XRD patterns (Figure 1), in which the profile shape of peaks for the products without [BMIM]Br are sharper than that with [BMIM]Br. The ratios of relative intensities of (100)/(101) diffraction, reflecting the degree of preferred growth orientation, are 0.98 without [BMIM]Br and 0.74 with [BMIM]Br, respectively. This small ratio can

Scheme 1. Illustration of Synthetic Procedures for Ionic Liquid [BMIM]Br

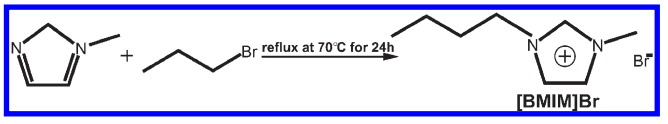

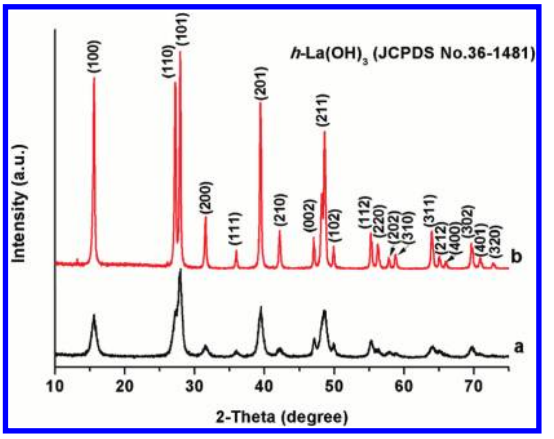

Figure 1. XRD patterns of *h*-$La(OH)_3$ under hydrothermal conditions at 200 °C for 8 h: (a) with [BMIM]Br (0.01 M, 1.5 mL); (b) without [BMIM]Br.

Table 1. Summary of the Synthesis of Typical Products under Various Experimental Parameters

sample	[BMIM]Br (0.01 M, 1.5 mL)	*T* (°C)	*t* (h)	heat-treatment	phase	morphology
Sample 1	√	200	1	/	*h*-$La(OH)_3$	nanoparticles
Sample 2	√	200	4	/	*h*-$La(OH)_3$	nanoparticles and nanorods
Sample 3	√	200	8	/	*h*-$La(OH)_3$	nanowires
Sample 4	√	200	12	/	*h*-$La(OH)_3$ and *m*-$LaVO_4$	nanowires
Sample 5	√	200	16	/	main *m*-$LaVO_4$	nanowires
Sample 6	√	200	32	/	main *m*-$LaVO_4$	nanowires
Sample 7	√	200	48	/	main *m*-$LaVO_4$	nanowires
Sample 8	√	200	48	600 °C for 12 h in air condition	pure *m*-$LaVO_4$	nanowires

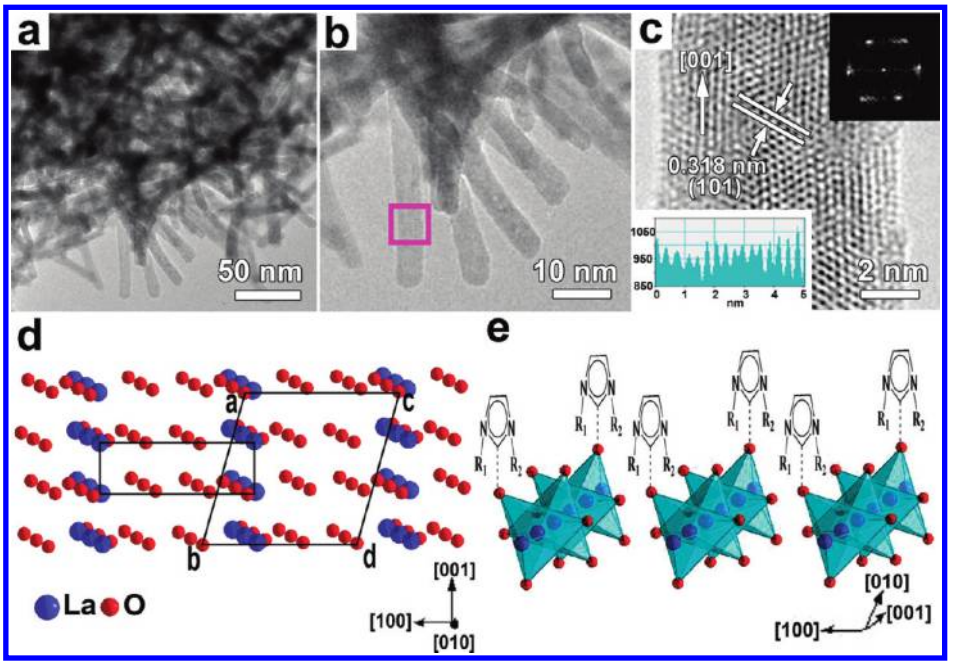

Figure 2. (a) TEM and (b, c) HRTEM images of *h*-$La(OH)_3$ nanowires obtained by the hydrothermal method with 1.5 mL of ionic liquid [BMIM]Br (0.01 M) at 200 °C for 8 h. The inset in (c) gives the fast Fourier transformation (FFT) pattern and the line profile from the digitalized HRTEM image, suggesting the nanowires grow as single-crystalline *h*-$La(OH)_3$. (d) Surface structure of *h*-$La(OH)_3$ along the [010] direction and schematic illustration of *h*-$La(OH)_3$ (010)-p(3 × 1)-$[BMIM]^+$ original cell. Moreover, $[BMIM]^+$ ions locate in the a−d sites, whereas $[BMIM]^+$ units are omitted for clarity. The rectangle represents a *h*-$La(OH)_3$ cell. (e) Schematic diagram of the preferential adsorption of $[BMIM]^+$ ions on the (010) plane for *h*-$La(OH)_3$ to form a tight coverage layer via the original cell.

be attributed to strengthen the 1D growth habit of *h*-$La(OH)_3$ along the [001] direction via [BMIM]Br. Therefore, the analyses demonstrate that the universality of ILs adsorbing model on the surface of materials to control the oriented growth is firmly accepted.

For the generation of 1D nanostructures through topotactic transformation in the reported references, one- or two-pot syntheses of simple compounds are required.[18] A one-pot approach containing the precursor synthesis and the topotactic transformation is undoubtedly more efficient.[19] Actually, $La(OH)_3$ is easily generated under normal temperature and pressure due to the very low solubility product constant ($K_{sp} = 2.0 \times 10^{-19}$). Moreover, no $LaVO_4$ precipitation was obtained when $La(NO_3)_3$ and NH_4VO_3 solutions were directly mixed. Herein, we design and synthesize $LaVO_4$ via a one-pot method in the $La(NO_3)_3$-NH_4VO_3-NaOH-[BMIM]Br-H_2O system. As shown in Table 1 and Figures 3 and 4, the products were pure *h*-$La(OH)_3$ without the formation of *m*-$LaVO_4$ during the reaction at 200 °C for 1−8 h. With a prolonged reaction time of 12−48 h, *m*-$LaVO_4$ began to appear, and then became the main product with the decrease of *h*-$La(OH)_3$. During the topotactic transformation from *h*-$La(OH)_3$ to *m*-$LaVO_4$, the interdiffusion of VO_3^- in the interlayer space of *h*-$La(OH)_3$ is a crucial step in controlling the phases of products, which is similar to the previous references for synthesizing Bi_2S_3[15] and Co_3O_4[18b] nanostructures. Overall, an one-pot method was established to prepare *m*-$LaVO_4$ with a complex structure through topotactic transformation from the *h*-$La(OH)_3$ precursor.

Figure 5a−c is typical TEM/HRTEM images of as-synthesized *m*-$LaVO_4$ through a one-pot hydrothermal approach with 1.5 mL of ionic liquid [BMIM]Br (0.01 M) at 200 °C for 48 h. The product consists of nanowires with uniform diameters varying from 10 to 12 nm (Figure 5a,b),

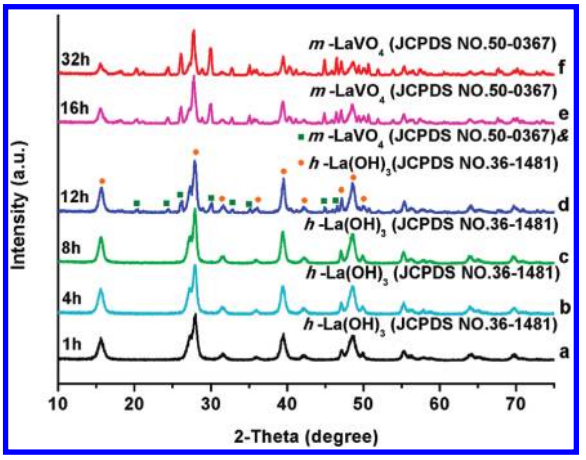

Figure 3. XRD patterns of samples synthesized with 1.5 mL of [BMIM]Br (0.01 M) at 200 °C for various dwell time: (a) 1 h, *h*-$La(OH)_3$; (b) 4 h, *h*-$La(OH)_3$; (c) 8 h, *h*-$La(OH)_3$; (d) 12 h, the mixture of *h*-$La(OH)_3$ and *m*-$LaVO_4$; (e) 16 h, main *m*-$LaVO_4$; and (f) 32 h, main *m*-$LaVO_4$.

while their lengths are in the range of about 10−12 μm (see Figure S2 in the Supporting Information). An HRTEM image (Figure 5c) shows that certain dislocations[20] are distributed homogeneously on the surface of nanowires, which is probably caused by a little of residual [BMIM]Br on its surface. The evidence is proved by Fourier transform infrared (FT-IR) spectrum (see Figure S3 in the Supporting Information). Structurally, most of the XRD peaks can be readily indexed to a monoclinic phase of $LaVO_4$ (JCPDS No. 50-0367), although three peaks marked with blue squares indicate traces of unidentified impurity (see Figure S4 in the Supporting Information). When the amount of ionic liquid [BMIM]Br is a lower or higher value (0.75 mL, 3.0 mL)

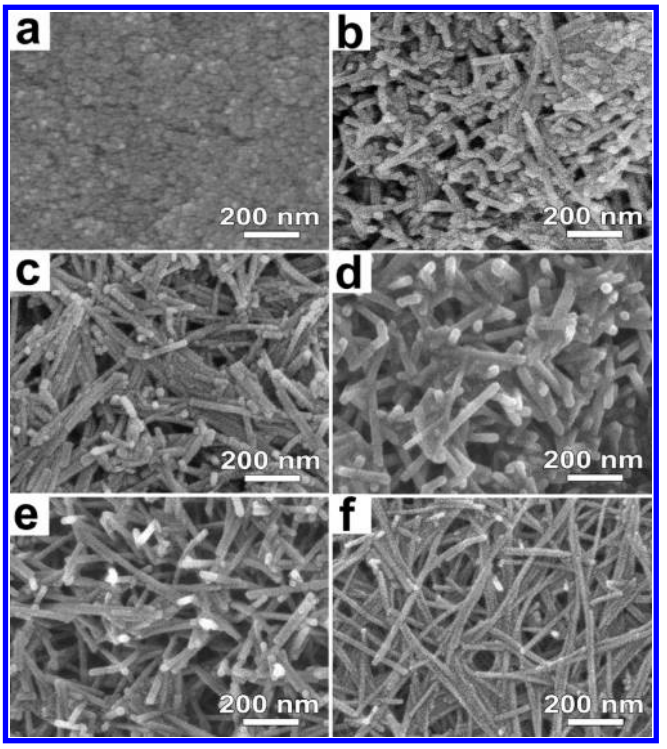

Figure 4. SEM images of the as-synthesized samples obtained at different reaction time with the same hydrothermal temperature of 200 °C and 1.5 mL of [BMIM]Br (0.01 M): (a) 1 h, *h*-$La(OH)_3$ nanoparticles; (b) 4 h, *h*-$La(OH)_3$ nanoparticles and nanorods; (c) 8 h, *h*-$La(OH)_3$ nanowires; (d) 12 h, the mixture of *h*-$La(OH)_3$ and *m*-$LaVO_4$ nanowires; (e) 16 h, main *m*-$LaVO_4$ nanowires; and (f) 32 h, ultralong *m*-$LaVO_4$ nanowires.

without other parameters being modified (Table S1, Supporting Information), *h*-$La(OH)_3$ or the mixture of *h*-$La(OH)_3$ and *m*-$LaVO_4$ nanowires are obtained as illustrated in Figure S5-6 (see the Supporting Information). In addition, experiments in several reaction temperatures with 1.5 mL of [BMIM]Br are systematically performed to investigate the variation on the microstructure of products in Figure S7-8 (see the Supporting Information). The lower temperatures of 80−150 °C favor the formation of *h*-$La(OH)_3$ nanoparticles, while the higher temperatures (180 °C and 220 °C) generally produce a mixture of *h*-$La(OH)_3$ and m-$LaVO_4$ nanowires. In a word, the addition of 1.5 mL of ionic liquid [BMIM]Br and the hydrothermal temperature of 200 °C are the optimized conditions to get ultralong *m*-$LaVO_4$ nanowires with a small quantity of impurities.

To decrease the content of residual IL and purify the products, heat-treatment of *m*-$LaVO_4$ obtained by hydrothermal method (200 °C, 48 h, 1.5 mL [BMIM]Br (0.01 M)) was performed at 600 °C for 12 h in air. The XRD pattern (Figure 5d) indicates that all the diffraction peaks are in good agreement with the standard values for *m*-$LaVO_4$ (JCPDS No. 50-0367, space group: $P21/n$ (No. 14)). The diameter and length of *m*-$LaVO_4$ nanowires (Figure 5e,f) are similar to that of the hydrothermal sample. Surprisingly, the dislocations on the surface of nanowires disappear, making the surface of wires very smooth, which is ascribed to removal of the residual ionic liquid. From the HRTEM image of an individual nanowire (Figure 5g), the clear lattice fringes of *m*-$LaVO_4$ nanowires can be seen with a *d*-spacing of 0.319 nm in accordance with the distance between (120) lattice planes, suggesting that the nanowires grow along the [010] direction.

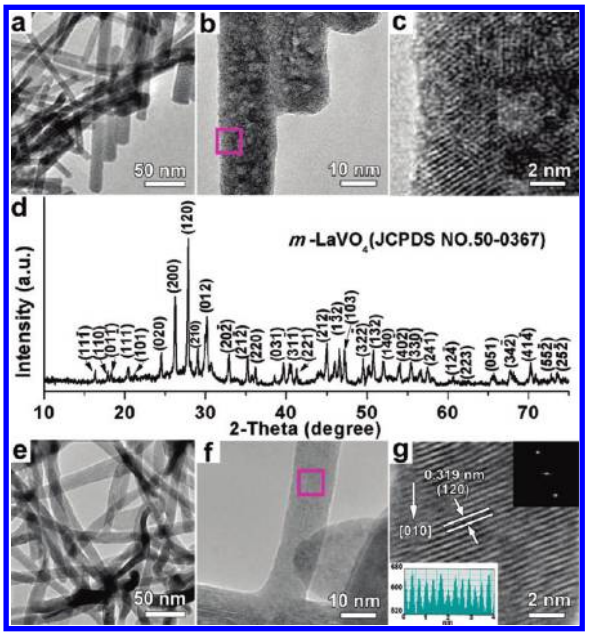

Figure 5. (a) TEM and (b, c) HRTEM images of *m*-$LaVO_4$ nanowires obtained under hydrothermal conditions with 1.5 mL of [BMIM]Br (0.01 M) at 200 °C for 48 h. (d) XRD pattern of *m*-$LaVO_4$ nanowires after heat-treatment at 600 °C for 12 h. (e) TEM and (f) HRTEM images of *m*-$LaVO_4$ nanowires after heat-treatment at 600 °C for 12 h. (g) HRTEM image of the selected area marked with a pink square in (f). The top inset in (g) shows the corresponding FFT pattern of *m*-$LaVO_4$ nanowires, while the bottom inset shows the line profile of an ordered region in (g), suggesting the interlayer distance of 0.319 nm.

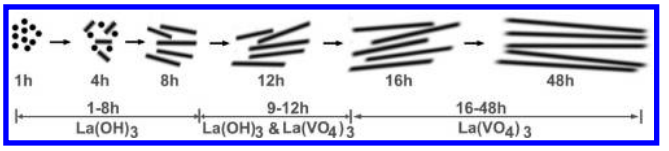

Figure 6. Schematic representation of the formation mechanism of *m*-$LaVO_4$ nanowires. The diagram displays the variation of the phases and morphologies of products with different reaction time.

The FFT analysis of the top inset in Figure 5g indicates the single-crystal nature of $LaVO_4$ with monoclinic structure.

3.2. Growth Mechanism of *m*-$LaVO_4$ Nanowires. On the basis of the experimental results, the whole process for the formation of *m*-$LaVO_4$ nanowires can be schematically illustrated in Figure 6. In the early stage, the intermediate products indicate the coexistence of *h*-$La(OH)_3$ nanorods and nanoparticles. As the reaction continued, it can be noted that the nanoparticles gradually disappear with the dramatically increase in the production of *h*-$La(OH)_3$ nanowires. For the transformation process from *h*-$La(OH)_3$ nanowires to *m*-$LaVO_4$ nanowires during 12 to 48 h, we attempt to understand this interesting phenomenon by topotactic transformation on a crystallographic view. The perspective views of *h*-$La(OH)_3$ along the *c* axis and of *m*-$LaVO_4$ along the *b* axis are presented in Figure 7 panels a and b, respectively. From Figure 7a, the planar triangles of *h*-$La(OH)_3$ along the *c* axis are arranged in a chain-like structure with a relatively larger spacing of 0.65 nm between the chains. At the vertical direction of the *c* axis, $La(OH)_3$ planar triangles in the same plane present a rhombus array, which is composed of four La atoms. Obviously, the La atoms of *m*-$LaVO_4$ marked with black parallelograms in the same planes (Figure 7b) also

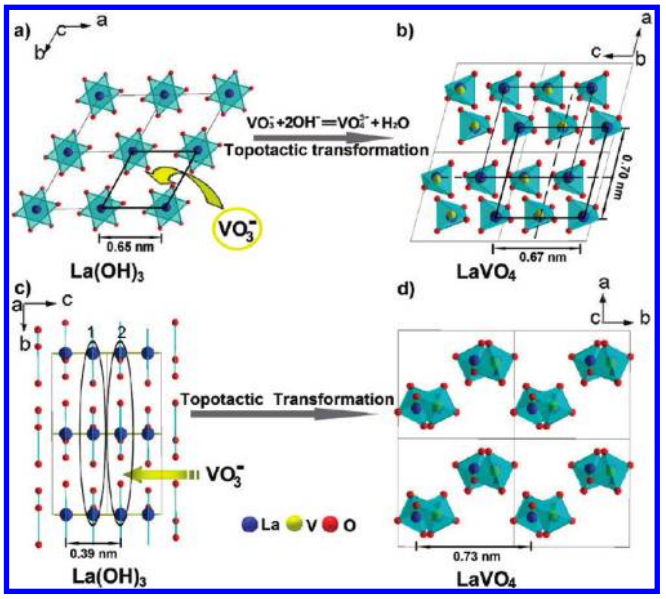

Figure 7. Illustrative crystal structure models of the topotactic transformation from *h*-$La(OH)_3$ to *m*-$LaVO_4$ along different directions. Crystallographic views with a similar rhombus array in (a) *h*-$La(OH)_3$ along the *c* axis, and (b) *m*-$LaVO_4$ along the *b* axis. Panels (c, d) represent the array periods of *h*-$La(OH)_3$ and *m*-$LaVO_4$ with layered structures, respectively.

have a rhombus array similar to that of *h*-$La(OH)_3$. Comparing the structures of *m*-$LaVO_4$ with *h*-$La(OH)_3$, tow rows of La atoms (located in the dashed line) are moved into the interchain areas of *h*-$La(OH)_3$ crystal without involving a larger change of the rhombus arrays of La atoms in the same planes. The perspective views on the other directions can clearly explain why the shifted La atoms are in the interchain positions of *h*-$La(OH)_3$ to form *m*-$LaVO_4$. The array periods of La atoms for *m*-$LaVO_4$ along the *b* axis (Figure 7d) is about 2-fold of that of *h*-$La(OH)_3$ along the *c* axis (Figure 7c), indicating that La atoms denoted 1 and 2 of *h*-$La(OH)_3$ have relatively upper and lower shifts from the $La(OH)_3$ planar triangles chains to the interchain with simultaneous diffusion of VO_3^- ions. As a result, the *b*-axis of *m*-$LaVO_4$ is consistent with the *c*-axis of *h*-$La(OH)_3$, which is supported by the analysis of their HRTEM images (Figures 2c and 5g). Thus, topotactic transformation is a plausible explanation of the transformation from single-crystalline *h*-$La(OH)_3$ nanowires to ultralong *m*-$LaVO_4$ nanowires.

4. Conclusion

In summary, single-crystalline *h*-$La(OH)_3$ nanowires have been successfully synthesized by an ionic liquid-assisted hydrothermal method at 200 °C for 8 h. The ionic liquid [BMIM]Br can vertically adsorb on the (010) plane of the $La(OH)_3$ crystal to form an absorption model for controlling the 1D oriented growth of the products. Ultralong *m*-$LaVO_4$ wire-like nanostructures were prepared from *h*-$La(OH)_3$ nanowires with the diffusion of VO_3^- ions through the topotactic transformation during 12−48 h. This research indicates that topotactic transformation may allow the design and fabrication of metal vanadates with 1D shapes from the corresponding metal hydroxide, and could be extended to the synthesis of nanoscale compounds with multicomponent and complex structures.

Acknowledgment. This work was supported by the National Natural Science Fundamental of China (Grand No. 20571044 and No. 20971070) and the Project Fundamental and Applied Research of Tianjin, China.

Supporting Information Available: SEM images of the as-obtained *h*-$La(OH)_3$ rod-like product through hydrothermal technology without [BMIM]Br at 200 °C for 8 h. SEM images of *m*-$LaVO_4$ obtained with the addition of ionic liquid [BMIM]Br (1.5 mL, 0.01 M) at 200 °C for 48 h: (a) low magnification and (b) high magnification. FT-IR spectrum of *m*-$LaVO_4$ synthesized by the hydrothermal method with the addition of ionic liquid [BMIM]Br (1.5 mL, 0.01 M) at 200 °C for 48 h. XRD pattern of *m*-$LaVO_4$ prepared under hydrothermal conditions with the addition of [BMIM]Br (1.5 mL, 0.01 M) at 200 °C for 48 h. Table S1. The summary of the synthesis of samples obtained under different amounts of ionic liquid [BMIM]Br and hydrothermal temperatures. XRD patterns of products synthesized with various amounts of ionic liquid [BMIM]Br (0.01 M) at 200 °C for 48 h: (a) 0.75 mL, *h*-$La(OH)_3$, and (b) 3.0 mL, the mixture of *h*-$La(OH)_3$ and *m*-$LaVO_4$. SEM images of products obtained with different amounts of ionic liquid [BMIM]Br (0.01 M) at 200 °C for 48 h: (a) 0.75 mL, *h*-$La(OH)_3$ nanowires; (b) 3.0 mL, the mixture of *h*-$La(OH)_3$ and *m*-$LaVO_4$ nanowires. XRD patterns of products fabricated under varied hydrothermal temperatures with 1.5 mL of [BMIM]Br (0.01 M) for 48 h: (a) 80 °C, *h*-$La(OH)_3$; (b) 100 °C, *h*-$La(OH)_3$; (c) 120 °C, *h*-$La(OH)_3$; (d) 150 °C, *h*-$La(OH)_3$; (e) 180 °C, the mixture of *h*-$La(OH)_3$ and *m*-$LaVO_4$; (f) 220 °C, the mixture of *h*-$La(OH)_3$ and *m*-$LaVO_4$. SEM images of products prepared under different temperatures with 1.5 mL of [BMIM]Br (0.01 M) for 48 h: (a) 80 °C, *h*-$La(OH)_3$ nanoparticles; (b) 100 °C, *h*-$La(OH)_3$ nanoparticles; (c) 120 °C, *h*-$La(OH)_3$ nanoparticles; (d) 150 °C, *h*-$La(OH)_3$ nanoparticles; (e) 180 °C, the mixture of *h*-$La(OH)_3$ and *m*-$LaVO_4$ nanowires; (f) 220 °C, the mixture of *h*-$La(OH)_3$ and *m*-$LaVO_4$ nanowires. These materials are available free of charge via the Internet at http://pubs.acs.org.

References

(1) (a) Xia, Y. N.; Yang, P. D.; Sun, Y. G.; Wu, Y. Y.; Mayers, B.; Gates, B.; Yin, Y. D.; Kim, F.; Yan, H. Q. *Adv. Mater.* **2003**, *15*, 353. (b) Chang, Y.; Zeng, H. C. *Cryst. Growth Des.* **2004**, *4*, 397. (c) Wang, Z. H.; Wang, L. L.; Wang, H. *Cryst. Growth Des.* **2008**, *8*, 4415.
(2) (a) Zhou, Y.; Antonietti, M. *Adv. Mater.* **2003**, *15*, 1452. (b) Antonietti, M.; Kuang, D. B.; Smarsly, B.; Zhou, Y. *Angew. Chem., Int. Ed.* **2004**, *43*, 4988. (c) Wang, W. W.; Zhu, Y. J. *Cryst. Growth Des.* **2005**, *5*, 505. (d) Li, Z. H.; Shkilnyy, A.; Taubert, A. *Cryst. Growth Des.* **2008**, *8*, 4526. (e) Lian, J. B.; Duan, X. C.; Ma, J. M.; Peng, P.; Kim, T.; Zheng, W. J. *ACS Nano* **2009**, *3*, 3749.
(3) (a) Zhou, Y.; Schattka, J. H.; Antonietti, M. *Nano Lett.* **2004**, *4*, 477. (b) Zhou, Y. *Curr. Nanosci.* **2005**, *1*, 35.
(4) Zheng, W. J.; Liu, X. D.; Yan, Z. Y.; Zhu, L. J. *ACS Nano* **2009**, *3*, 115.
(5) (a) Zhang, S. Y.; Li, W. Y.; Li, C. S.; Chen, J. *J. Phys. Chem. B* **2006**, *110*, 24855. (b) Chen, L.; Jiang, F. L.; Wu, M. Y.; Li, N.; Xu, W. T.; Yan, C. F.; Yue, C. Y.; Hong, M. C. *Cryst. Growth Des.* **2008**, *8*, 4092. (c) Ng, S. H.; Tran, N.; Bramnik, K. G.; Hibst, H.; Novák, P. *Chem.—Eur. J.* **2008**, *14*, 11141. (d) Zhao, Y.; Xie, Y.; Zhu, X.; Yan, S.; Wang, S. X. *Chem.—Eur. J.* **2008**, *14*, 1601. (e) Ma, H.; Zhang, S. Y.; Ji, W. Q.; Tao, Z. L.; Chen, J. *J. Am. Chem. Soc.* **2008**, *130*, 5361.
(6) Kudo, A.; Omori, K.; Kato, H. *J. Am. Chem. Soc.* **1999**, *121*, 11459.
(7) (a) Huignard, A.; Gacoin, T.; Boilot, J. P. *Chem. Mater.* **2000**, *12*, 1090. (b) Peng, B.; Fan, Z. C.; Qiu, X. M.; Jiang, L.; Tang, G. H.; Ford, H. D.; Huang, W. *Adv. Mater.* **2005**, *17*, 857. (c) Stouwdam, J. W.; Raudsepp, M.; van Veggel, F. C. J. M. *Langmuir* **2005**, *21*, 7003. (d) Pan, G. H.; Song, H. W.; Bai, X.; Fan, L. B.; Yu, H. Q.; Dai, Q. L.; Dong, B.; Qin, R. F.; Li, S. W.; Lu, S. Z.; Ren, X. G.; Zhao, H. F. *J. Phys. Chem. C* **2007**, *111*, 12472. (e) Yu, H. Q.; Song, H. W.; Pan, G. H.; Qin, R. F.; Fan, L. B.; Zhang, H.; Bai, X.; Li, S. W.; Zhao, H. F.; Lu, S. Z. *J. Nanosci. Nanotechnol.* **2008**, *8*, 1432.
(8) Liang, Y. C.; Hong, M. C.; Su, W. P.; Cao, R.; Zhang, W. J. *Inorg. Chem.* **2001**, *40*, 4574.
(9) Oka, Y.; Yao, T.; Yamamoto, N. *J. Solid State Chem.* **2000**, *152*, 486.
(10) (a) Jia, C. J.; Sun, L. D.; You, L. P.; Jiang, X. C.; Luo, F.; Pang, Y. C.; Yan, C. H. *J. Phys. Chem. B* **2005**, *109*, 3284. (b) Fan, W. L.;

Song, X. Y.; Bu, Y. X.; Sun, S. X.; Zhao, X. *J. Phys. Chem. B* **2006**, *110*, 23247. (c) Liu, J. F.; Li, Y. D. *Adv. Mater.* **2007**, *19*, 1118. (d) Liu, J. F.; Li, Y. D. *J. Mater. Chem.* **2007**, *17*, 1797. (e) Liu, J. F.; Chen, W.; Liu, X. W.; Zhou, K. B.; Li, Y. D. *Nano Res.* **2008**, *1*, 46.
(11) Fan, W. L.; Zhao, W.; You, L. P.; Song, X. Y.; Zhang, W. M.; Yu, H. Y.; Sun, S. X. *J. Solid State Chem.* **2004**, *177*, 4399.
(12) Fan, W. L.; Song, X. Y.; Sun, S. X.; Zhao, X. *J. Solid State Chem.* **2007**, *180*, 284.
(13) Yu, C. C.; Yu, M.; Li, C. X.; Zhang, C. M.; Yang, P. P.; Lin, J. *Cryst. Growth Des.* **2009**, *9*, 783.
(14) Ma, J.; Wu, Q. S.; Ding, Y. P. *J. Nanopart. Res.* **2008**, *10*, 775.
(15) Li, L. S.; Sun, N. J.; Huang, Y. Y.; Qin, Y.; Zhao, N. N.; Gao, J.; Li, M. X.; Zhou, H. H.; Qi, L. M. *Adv. Funct. Mater.* **2008**, *18*, 1194.
(16) Malham, I. B.; Letellier, P.; Turmine, M. *J. Phys. Chem. B* **2006**, *110*, 14212.
(17) (a) Yaghi, O. M.; Li, G. M.; Li, H. L. *Nature* **1995**, *378*, 703. (b) Jin, J.; Iyoda, T.; Cao, C. S.; Song, Y. L.; Jiang, L.; Li, T. J.; Zhu, D. B. *Angew. Chem., Int. Ed.* **2001**, *40*, 2135.
(18) (a) Gates, B.; Mayer, B.; Wu, Y. Y.; Sun, Y. G.; Cattle, B.; Yang, P. D.; Xia, Y. N. *Adv. Funct. Mater.* **2002**, *12*, 679. (b) Lou, X. W.; Deng, D.; Lee, J. Y.; Feng, J.; Archer, L. A. *Adv. Mater.* **2008**, *20*, 258.
(19) Zhang, D. H.; Li, G. D.; Li, J. X.; Chen, J. S. *Chem. Commun.* **2008**, *29*, 3414.
(20) Liu, Y. D.; Zhang, Y.; Wu, G. Z.; Hu, J. *J. Am. Chem. Soc.* **2006**, *128*, 7456.